



Strain- or Stress-Sensing in Mechanochemical Patterning by the Phytohormone Auxin

Jean-Daniel Julien^{1,2,3}  · Alain Pumir^{1,2,3}  · Arezki Boudaoud¹ 

Received: 8 November 2017 / Accepted: 12 March 2019 / Published online: 22 March 2019
© Society for Mathematical Biology 2019

Abstract

Both chemical and mechanical fields are known to play a major role in morphogenesis. In plants, the phytohormone auxin and its directional transport are essential for the formation of robust patterns of organs, such as flowers or leaves, known as phyllotactic patterns. The transport of auxin was recently shown to be affected by mechanical signals, and conversely, auxin accumulation in incipient organs affects the mechanical properties of the cells. The precise interaction between mechanical fields and auxin transport, however, is poorly understood. In particular, it is unknown whether transport is sensitive to the strain or to the stress exerted on a given cell. Here, we investigate the nature of this coupling with the help of theoretical models. Namely, we introduce the effects of either mechanical stress or mechanical strain in a model of auxin transport and compare the patterns predicted with available experimental results, in which the tissue is perturbed by ablations, chemical treatments, or genetic manipulations. We also study the robustness of the patterning mechanism to noise and investigate the effect of a shock that changes abruptly its parameters. Although the model predictions with the two different feedbacks are often indistinguishable, the strain feedback seems to better agree with some of the experiments. The computational modeling approach used here, which enables us to distinguish between several possible mechanical feedbacks, offers promising perspectives to elucidate the role of mechanics in tissue development, and may help providing insight into the underlying molecular mechanisms.

Keywords Patterning · Chemomechanical model · Auxin transport · Shoot apical meristem

Electronic supplementary material The online version of this article (<https://doi.org/10.1007/s11538-019-00600-5>) contains supplementary material, which is available to authorized users.

✉ Arezki Boudaoud
arezki.boudaoud@ens-lyon.fr

Extended author information available on the last page of the article

1 Introduction

Understanding the formation of patterns in living organisms has long intrigued scientists (Adler et al. 1997). This phenomenon has been investigated in a wide variety of species, such as zebrafish (Kondo 2002) or hydra (Bode 2009). We focus here on patterning in plants. The highly regular positioning of the organs in plant shoots, called phyllotaxis, relies on the patterns of the phytohormone auxin, whose local accumulation is necessary for the emergence of new organs (Kuhlemeier and Reinhardt 2001, Heisler et al. 2005). Auxin efflux is facilitated by the membrane-localized PIN FORMED1 (PIN1) protein (Palme and Gälweiler 1999, Vernoux et al. 2000), which can be polarly (asymmetrically) distributed, inducing a directional transport of auxin, and resulting in well-defined auxin patterns. This transport is essential for the development of the plant. Indeed, knocking down the transporter activity, either genetically or chemically, leads to the absence of organ primordia at the shoot tip. Organ development can be then rescued by local application of exogenous auxin (Okada et al. 1991; Reinhardt et al. 2000, 2003).

Several models have been proposed to describe the interaction between the hormone and its carrier in the context of the shoot apex, with the major assumption that the transporters allocation between the different sides of a cell is driven by auxin fluxes (Stoma et al. 2008) or by auxin concentrations (Smith et al. 2006; Jönsson et al. 2006; Sahlin et al. 2009; Smith and Bayer 2009). Here, we focus on the second assumption, which has received more attention, because how the auxin concentration regulates the transporters remains unclear.

Since morphogenesis relies on changes in the structural elements of the organism, biochemical patterns must also influence the mechanics of these structural elements, in plants (Hamant and Traas 2010) and in animals (Howard et al. 2011; Davidson 2011; Rauzi and Lenne 2011). Conversely, mechanics can feed back on biochemical processes (Hamant and Traas 2010; Howard et al. 2011; Iskratsch et al. 2014; Sampathkumar et al. 2014), including gene expression (Fernández-Sánchez et al. 2015) and cell fate (Bellas and Chen 2014). Plants are well suited to study the coupling between biochemical and biophysical processes as hydrodynamic cell pressure generates tremendous forces and results in a high tension in the polysaccharide-based walls surrounding cells (Geitmann and Ortega 2009; Hamant and Traas 2010). Recent progress in computational approaches (Chickarmane et al. 2010) and in the measurements of cell mechanics (Milani et al. 2013) has fostered a renewed interest in the mechanics of plant morphogenesis.

Notably, at the shoot apex, organogenesis is associated with a decrease in the stiffness of the cell wall (Peaucelle et al. 2011) and likely with a reduced mechanical anisotropy (Sassi et al. 2014). In the context of phyllotaxis, the coupling between mechanics and chemistry was explored theoretically (Newell et al. 2008), and mechanics has been proposed to regulate the transport of auxin in the shoot apical meristem (Heisler et al. 2010). A mechanical feedback, capable of generating a local accumulation of auxin, was postulated (Heisler et al. 2010). Based on preferential localization of PIN1 in the regions of the plasma membrane in contact with the wall with highest mechanical stress, this mechanical feedback is supported by several experiments (Heisler et al. 2010; Nakayama et al. 2012; Braybrook and Peaucelle 2013). How-

ever, whether PIN1 polarity is driven by the stress or by the strain of the cell wall remains unclear. More generally, the issue of stress- or strain-sensing calls for further investigation, especially in the context of plant development (Mouliia et al. 2015).

Here, we address this issue by investigating a model of mechanical feedback on auxin transport, whose predictions can be compared with experimental results. We also study the robustness of the pattern formation mechanism with respect to noise and abrupt changes in some of the biochemical parameters. The predictions of the two mechanisms do not differ much. A feedback based on strain nonetheless leads to more realistic predictions, and to a patterning mechanism which is less sensitive to noisy inputs or sharp perturbations.

2 Results

2.1 A Mechanochemical Model of Auxin Patterning

We built a mechanochemical model of auxin transport and tissue mechanics that incorporates the influence of auxin on the stiffness of the cell wall and the mechanical feedback from the cell wall on auxin transport, as illustrated in Fig. 1a. We briefly describe its main ingredients here, deferring further details to the section ‘Model formulation’ below. We model a single cell layer, accounting for the epidermis of the shoot apex. We simplify tissue topology and assume the cells to form a regular hexagonal lattice, following Heisler et al. (2010), because we aim at stereotypic simulation results that would ease the comparison between strain- and stress-sensing mechanisms. The tissue is under global isotropic tension from turgor pressure, the cellular inner pressure that is assumed to be uniform. Each edge of the lattice is made of two contiguous cell walls associated with either of the two neighboring cells. Each cell wall is modeled by a linear spring, whose stiffness decreases with auxin concentration in the corresponding cell. This accounts for the positive effect of auxin on growth in the shoot apex. Changes in auxin concentration are due to production, degradation, diffusion and transport. We considered two hypotheses for the mechanical feedback: PIN1 transporters are inserted preferentially facing the cell walls that undergo (1) the highest elastic strain (elastic deformation) or (2) the highest stress (force).

We used two main observables: the polarity \mathcal{P} , defined as the ratio between the highest and the lowest transporter concentrations along the cell edges, and the membrane fraction \mathcal{F} , defined as the ratio between the number of transporters localized at the plasma membrane and the total amount of transporters in a cell (Fig. 1b). Typical patterns obtained by solving the models numerically are shown in Fig. 1c. In order to verify our simulations, we performed an analytical linear stability analysis of the homogeneous state (supplementary text and Fig. S1) and predicted wavelengths in agreement with numerical results for a broad range of parameter values.

For a given set of parameters, wavelengths are larger for strain- than for stress-sensing (in agreement with linear stability analysis, see the supplementary note and Fig. S1). Because of this discrepancy in the wavelength, all analyses performed hereafter were also carried out on four other sets of parameters for the stress feedback,

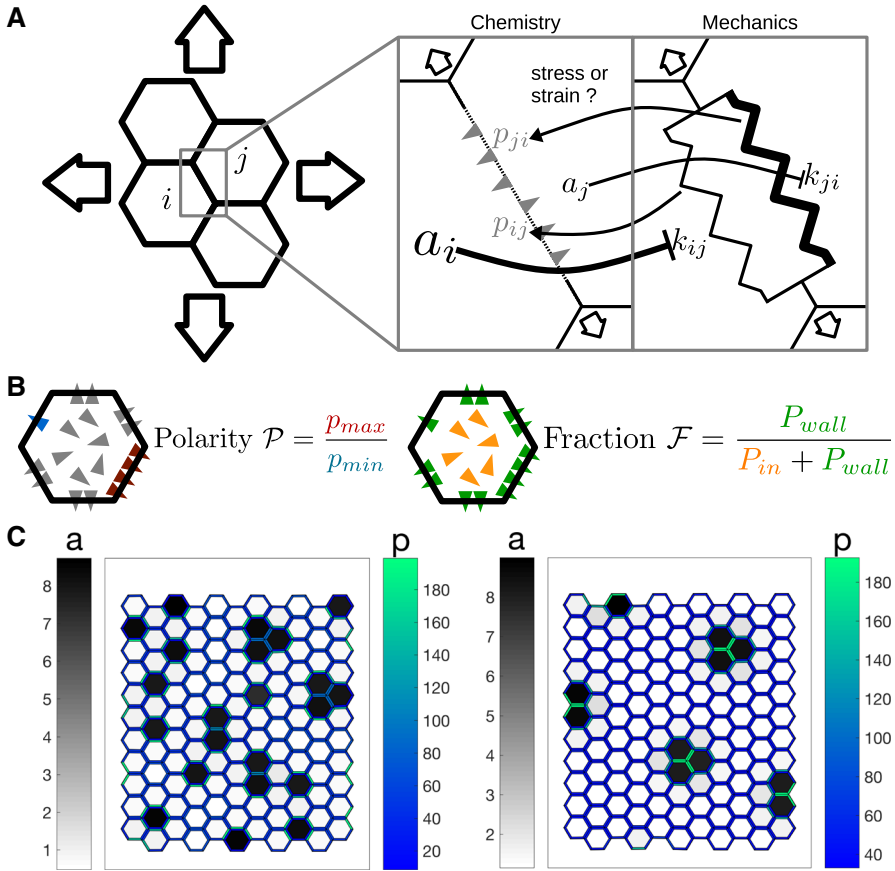


Fig. 1 Modeling assumptions and observables: **a** schematic of the model: The tissue consists of hexagonal cells. The auxin transporters are localized at the plasma membranes and are influenced by the mechanical status of the corresponding cells walls. The biochemical and mechanical effects are presented in two different boxes, and their interactions are represented by arrows. The tissue is stretched by the turgor pressure. PIN1 proteins facilitate auxin movement out of cells. The stiffness of each cell wall is a decreasing function of the auxin concentration in the cell. The amount of effective transporters increases with the stress or strain at the cell wall. **b** Schematic definition of the two observables: The triangles represent the PIN1 transporters, colored according to the definition of the observables. The polarity \mathcal{P} is the ratio between the two extremal concentrations in the cell walls of a cell. The fraction \mathcal{F} is the ratio between the number of effective transporters and the total number of transporters. **c** An example of pattern predicted by the model, with each feedback (left: stress; right: strain). The cells are colored according to their auxin concentration (gray levels) and the cell walls according to the density of PIN1 transporters (blue-green levels)

presented in the supplementary material (Fig. S2–6). These additional simulations largely support the conclusions presented here.

2.2 Cell Ablation Induces Radial Polarity

When a single epidermal cell is laser-ablated at the shoot apex, the hypothesis that the epidermis is in tension implies that the maximal stress orientation is circumferential

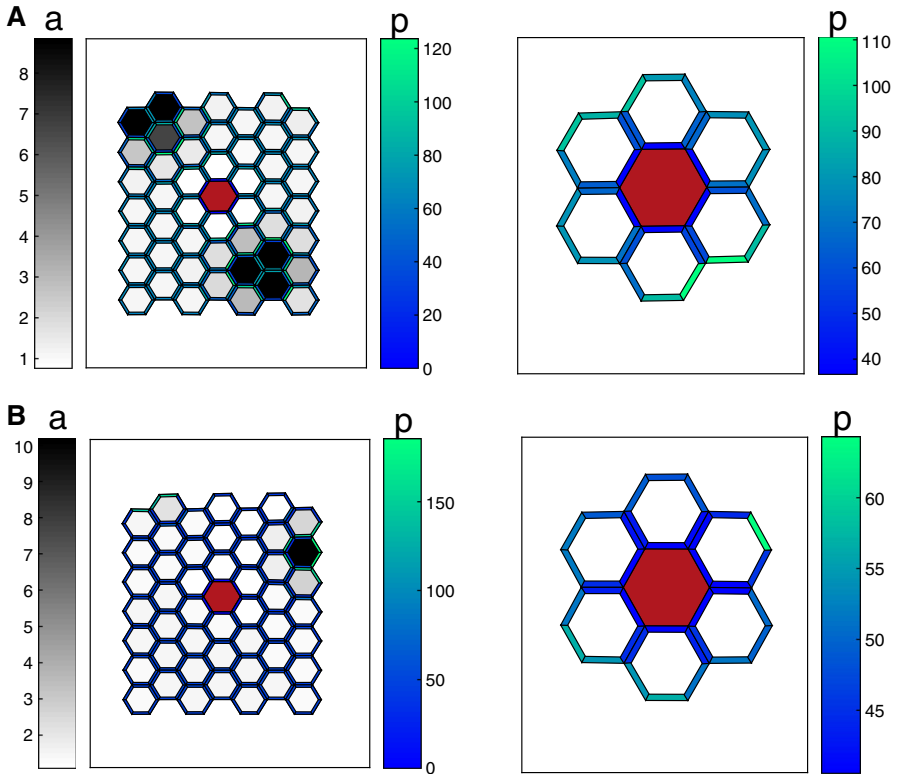


Fig. 2 Radial polarity around a cell ablation: The red hexagon corresponds to the ablated cell, whose walls, auxin, and transporters have been removed from the simulation. The transporters pointing toward this cell are also removed. The cells are colored according to their auxin concentration and the cell walls according to the concentration of transporters. The insertion of transporters is driven either by stress (a) or by strain (b). Auxin is not represented on the close-ups. Parameters for the strain feedback are indicated in Table 1. Parameters for the stress feedback are identical, except for $H_k = 1.06$, which was chosen to increase wavelength and better visualize the effect of an ablation on polarity. (Results are independent of the value of H_k .)

around the ablation (Hamant et al. 2008). The preferential localization of PIN1 transporters in the stretched walls would then makes the transport radial. A model similar to ours was able to reproduce this observation with a stress-driven feedback (Heisler et al. 2010). Here, we specifically asked whether our model can, with a strain-driven feedback mechanism, reproduce the experimental results. As in Heisler et al. (2010), we modeled the ablated cell by removing auxin, its transporters and cell walls, and by preventing the insertion of transporters in the membranes adjacent to ablated cells. Our results, see Fig. 2, show a radial reorientation of the transporters in neighboring cells, as observed in experiments (Heisler et al. 2010). It thus appears that ablation experiments do not allow us to distinguish between strain- and stress feedback mechanisms.

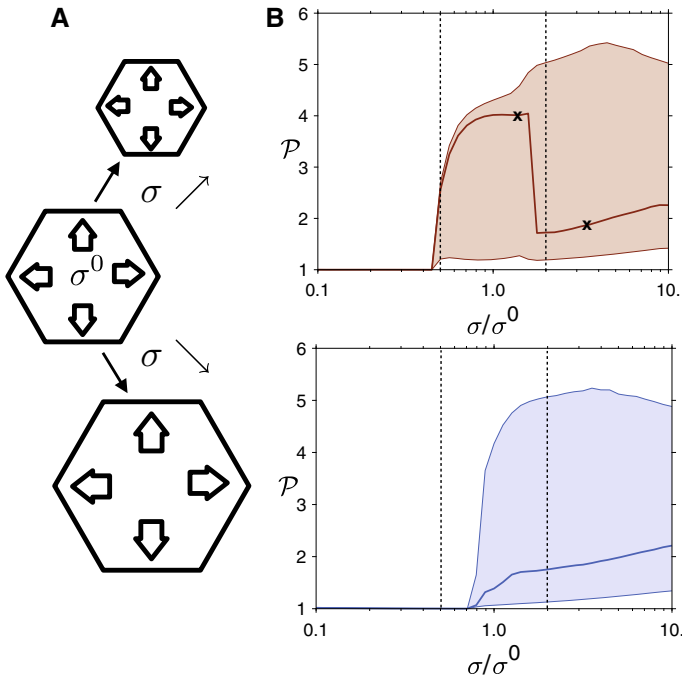


Fig. 3 Dependence of polarity on turgor pressure: **a** schematic of the simulations: Starting from σ^0 , the pressure is gradually increased or decreased, for pressures ranging from $0.1 \times \sigma^0$ and $10 \times \sigma^0$. **b** For each cell, the polarity \mathcal{P} is measured. The curves represent the median value of \mathcal{P} and the shaded areas in the interval between the 15th and 85th percentiles in a tissue of 3600 cells. The results are shown in red (left) for the stress-based feedback, in blue (right) for the strain-based feedback. The dashed lines show the range of pressure investigated experimentally (Nakayama et al. 2012) and the black crosses indicate the parameters for which tissues are shown in Fig. S8

2.3 Variations of Polarity with Turgor Pressure

Experiments with osmotic treatments show that PIN1 polarity \mathcal{P} is affected by changes in turgor pressure (Nakayama et al. 2012). By performing osmotic treatments, turgor pressure was varied by approximately a factor 2 in these experiments. Polarity was significantly smaller (−15%) with reduced turgor and slightly smaller (−5%) with enhanced turgor.

We simulated the effect of a gradual increase or decrease in turgor pressure by modulating tissue tension σ (see Eq.(1)) with respect to its reference value, σ and monitored the change in the polarity of the transporters with the two mechanical feedbacks. Our results, see Fig. 3, show that, irrespective of the feedback mechanism, polarity increases over a range $0.5\sigma^0 \lesssim \sigma \lesssim 2\sigma^0$, as observed experimentally.

The increase is sharper at small turgor pressure, consistent with experiments. At higher values of σ ($\sigma \approx 2\sigma^0$), the two models slightly disagree with experiments as they predict a slight increase in polarity, while a small decrease is observed. It is unclear whether this is due to a shortcoming of the model or to a bias in experimental quantifications.

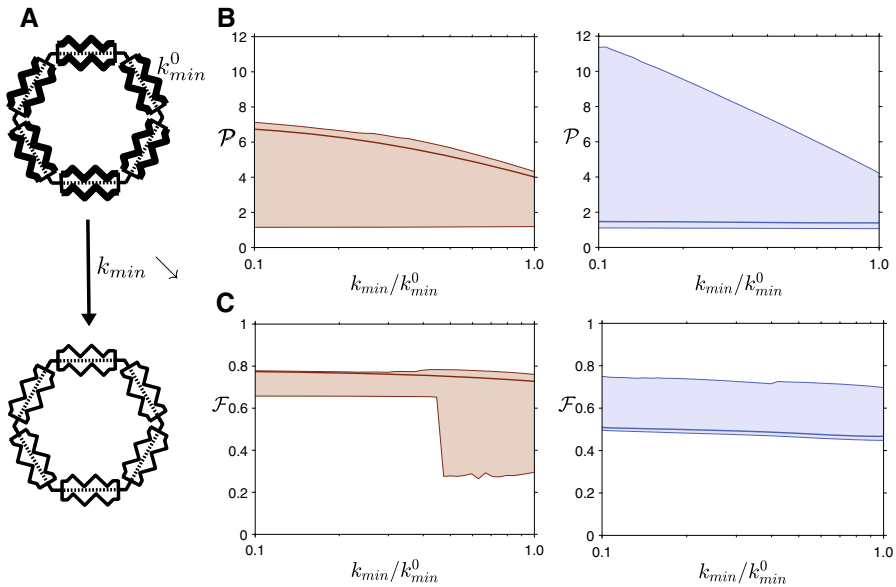


Fig. 4 Global softening of the tissue increases polarity: **a** schematic of the simulations: starting from k_{min}^0 , the minimal stiffness of the tissue is gradually decreased, ranging from k_{min}^0 to $k_{min}^0/10$. This corresponds to the stiffness at high levels of auxin. We quantified **b** the polarity \mathcal{P} and **c** the membrane fraction \mathcal{F} of transporters. The curves represent the median, and the shaded areas the interval between the 15th and 85th percentiles in a tissue of 3600 cells. The results are shown in red (left) for the stress-based feedback and in blue (right) for the strain-based feedback

With the stress feedback, the sharp drop seen in Fig. 3 is due to a change in the overall generated pattern of auxin peaks, which is not relevant in the present context, and is followed by an increase in polarity; Examples of tissues and PIN1 distributions before and after this transition are shown in Figure S2.

2.4 Global Softening of the Tissue Increases Polarity

Cellulose is the stiffest polysaccharide in plant cell walls. Accordingly, impairing cellulose synthesis by chemical treatments leads to the softening of plant tissues (Ryden et al. 2003). The consequence of such treatments on PIN1 localization was also investigated in Heisler et al. (2010). First, PIN1 polarity, \mathcal{P} , is amplified—the membrane concentration of PIN1 increases where it is high before treatment and decreases elsewhere. Second, the amount of PIN1 decreases in the cytosol, or equivalently the membrane fraction \mathcal{F} increases.

We simulated such treatments by decreasing the minimal stiffness, k_{min} , of the cell walls (Fig. 4). The increase in polarity \mathcal{P} and in the membrane fraction \mathcal{F} is reproduced with both feedbacks (Fig. 4). Therefore, these experiments do not allow us to discriminate between the two models of feedback.

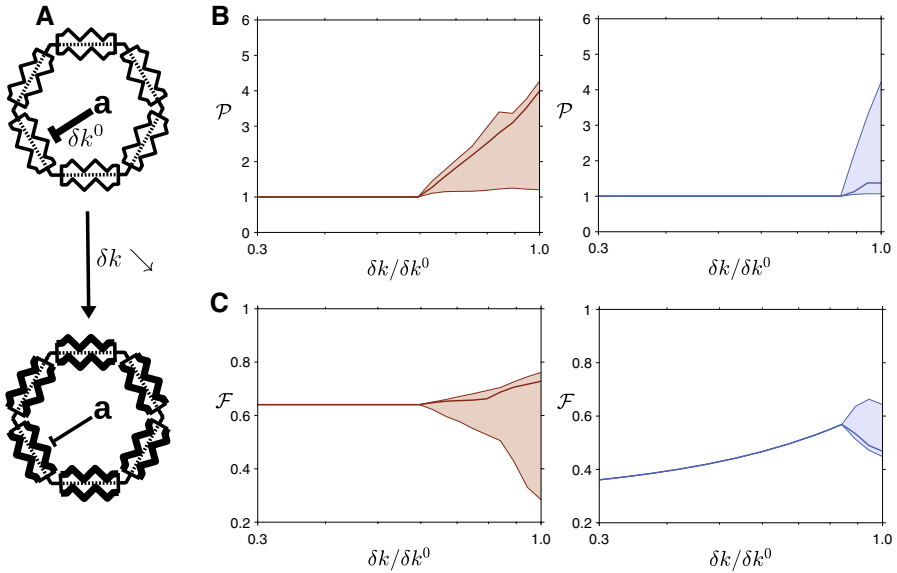


Fig. 5 Reducing auxin effects on the cell wall disrupts polarity: **a** schematic of the simulations: Starting from δk^0 , the amplitude of stiffness variations is gradually decreased, from k_{\min}^0 to $0.3 \times k_{\min}^0$. We quantified **b** the polarity \mathcal{P} and **c** the membrane fraction \mathcal{F} of transporters. The curves represent the median and the shaded areas the interval between the 15th and 85th percentiles in a tissue of 3600 cells. The results are shown in red (left) for the stress-based feedback and in blue (right) for the strain-based feedback

2.5 Reducing Auxin-Driven Softening Disrupts Polarity

It has been shown that de-methyl-esterification of the pectin homogalacturonan by pectin methyl-esterases (PMEs) is necessary for auxin to soften the cells (Peaucelle et al. 2008). Indeed, in plants overexpressing an inhibitor of PME activity, PME INHIBITOR3, patterns of auxin accumulation are absent and organ primordia do not form. In addition, the application of auxin does not trigger any of auxin response (no expression of the response reporter DR5), tissue softening or organ formation (Braybrook and Peaucelle 2013). In these plant lines, polarity and membrane fraction are both reduced.

To simulate such overexpression, we decreased the value of the parameter, δk that controls the sensitivity of cell wall stiffness to auxin, see Eq. (3) in the methods section. A vanishing δk means that auxin has no effect on wall stiffness, and high values of δk imply that a small change in auxin level induces a large change in stiffness. In parallel, we kept $k_{\min} + \delta k$ constant so that the reference stiffness in the absence of auxin remains unchanged. We measured the polarity \mathcal{P} and the fraction \mathcal{F} of transporters in the cell walls with the two types of feedbacks.

Figure 5 shows that when δk decreases, the polarity converges toward 1, corresponding to a homogeneous state with no patterns. Thus, the conclusion that the polarity is lost as a result of tissue stiffening is independent of the nature of the mechanical feedback. However, the variations of the membrane fraction \mathcal{F} depend on the pre-

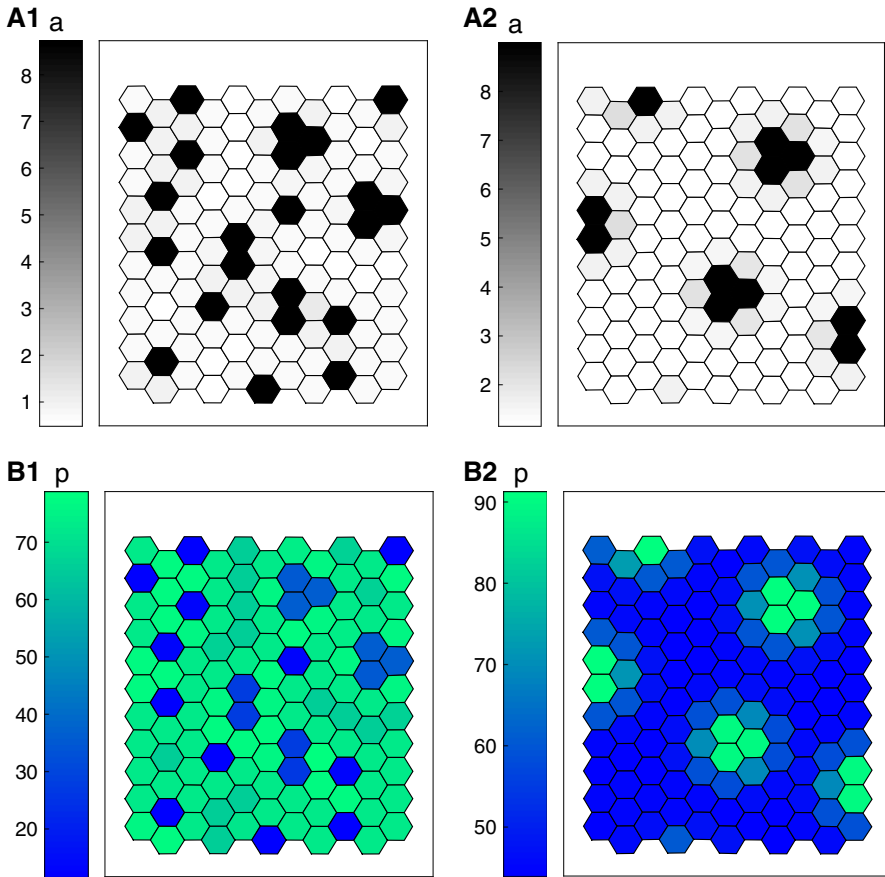


Fig. 6 Correlation between auxin and PIN1 concentrations: examples of pattern predicted by the model, with each feedback (**A/B1**: stress; **A/B2**: strain). The cells are colored according to their auxin concentration (gray levels, **A1/2**), or according to the density of PIN1 transporters, averaged over their walls (blue-green levels, **B1/2**)

cise feedback mechanism. When stiffening the tissue, \mathcal{F} decreases with the strain feedback, but remains approximately constant with the stress feedback, as shown in Fig. 5.

The behavior of the model can be understood analytically. In the homogeneous state, that is, in the absence of auxin patterns as observed in the simulations when δk is decreased, the membrane fraction can be computed exactly, as shown in the supplementary material. The calculations predict that $\mathcal{F}^{\text{stress}}$ remains constant, whereas $\mathcal{F}^{\text{strain}}$ decreases when δk decreases. Note that it is relevant to assume a homogeneous state of the system because naked meristems do not show auxin accumulation patterns. In view of these results, we conclude that a strain feedback is more realistic to describe experiments where PME activity is reduced.

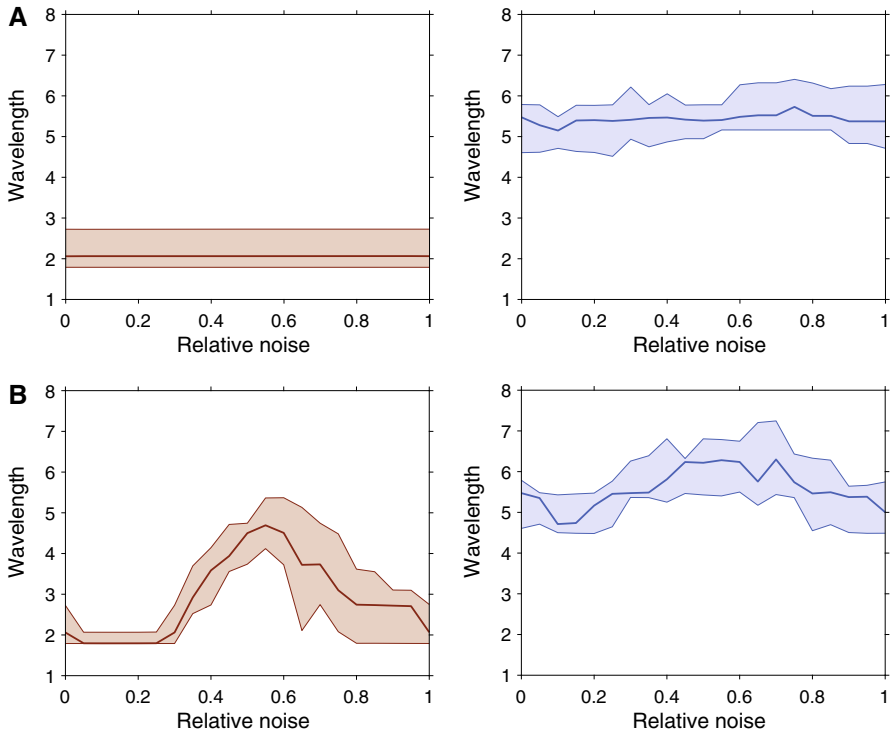


Fig. 7 Robustness to noise: The auxin production rate s_a (a) or the PIN1 concentration P (b) is spatially and temporally random, with a uniform distribution centered around the value of these parameters without noise. The relative noise amplitude is half the ratio between the width of this interval and the average value of the variable. The wavelength is measured as the average distance between a peak and its nearest neighbor. The prediction of the model with the stress feedback is shown in red (left), while the one with the strain feedback is represented in blue (right). The curves represent the median and the shaded areas the interval between the 15th and 85th percentiles

2.6 Correlation Between Auxin Level and Polarity

Experiments showed that, at the initiation of a primordia, the concentration of PIN1 transporters in the plasma membrane increases with the concentration of auxin (Heisler et al. 2005), likely independently of the increase in PIN1 transcription in response to auxin. Comparison of auxin and PIN1 concentrations in our simulations show that with the strain-sensing mechanism, the model qualitatively reproduces the experimental observations, whereas a stress-sensing mechanism leads to the opposite behavior, see Fig. 6. Again, analytical calculations in the limit of small auxin fluctuations around the homogeneous state confirm this result, regardless of the choice of parameters (see supplementary material). Accordingly, these results support a strain-sensing mechanism.

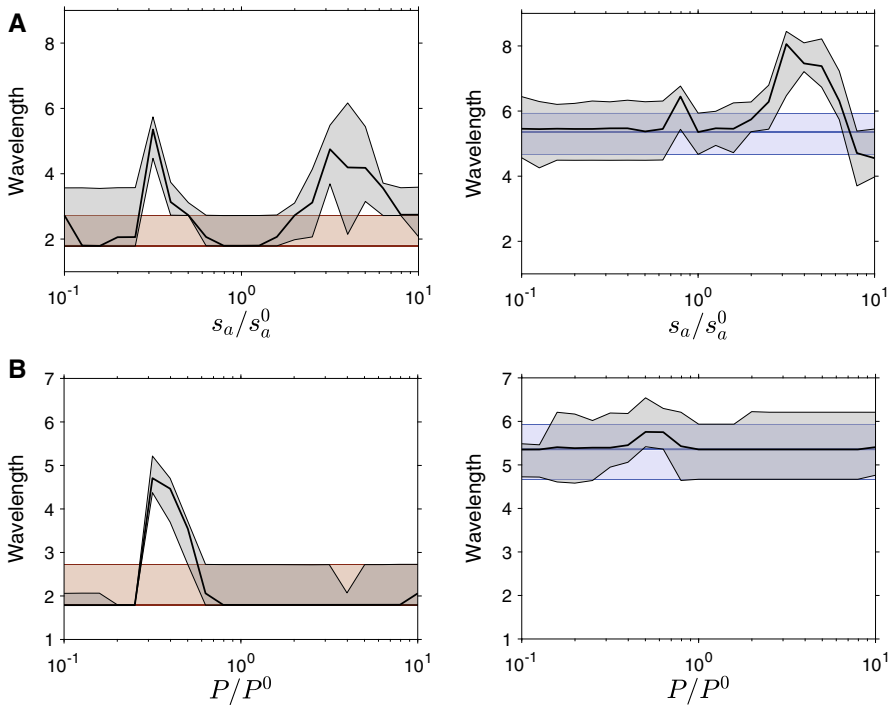


Fig. 8 Robustness to sharp variations: The auxin production rate s_a (a) or the PIN1 concentration P (b) is transiently modified over the entire tissue. Once the tissue reaches equilibrium, the original set of parameters is restored. The wavelength is measured at equilibrium before the shock and at equilibrium after resetting the original parameters. The wavelength before the shock is plotted in red for the stress feedback (left) and in blue for the strain feedback (right). The wavelength after the recovery is plotted in black. The curves represent the median, the red and blue shaded areas the interval between the 15th and 85th percentiles before the shock, and the black shaded areas the same percentiles after the resetting

2.7 Robustness to Noise

We now investigate the sensitivity of the pattern to noise. To this end, a random term, temporally and spatially uncorrelated, is added to the production rate of auxin or to the concentration of transporters, respectively s_a or P in Eq. (2). We measured the wavelength of the pattern and its dependence on the noise amplitude.

As shown by panel A in Fig. 7, the pattern is almost insensitive to the effect of noise on the production of auxin. In contrast, see Fig. 7b, noise in the concentration of transporters P alters significantly the pattern. With the stress feedback, the wavelength is observed to increase by up to 200%, whereas the increase in the wavelength of the pattern is only 20% with the strain feedback. This difference in the sensitivity of the patterns to noise in the transporters, PIN1, also discriminates between the two models. Although it is difficult to assess the level of noise in plants, the striking robustness of phyllotaxis to fluctuations in auxin levels (Vernoux et al. 2011) suggests that the feedback based on strain is more plausible.

2.8 Robustness to Sharp Variations

Even though robustness to noise discriminates between the two models, noise is difficult to manipulate experimentally. Robustness can also be tested by applying a transient shock to the system, i.e., a sharp modification of the external parameters, and by observing whether the tissue returns to its pre-shock state. Experimentally, this is feasible by transient chemical perturbation, such as external auxin application or inhibition of auxin transport, as performed in Heisler et al. (2005).

We simulated such perturbations as follows. In a tissue at equilibrium, we modified the mean auxin level $\langle a \rangle$ (through the production rate s_a , as shown in Fig. 8a) or the concentration of transporters P , as shown in Fig. 8b, and let the system reach a new equilibrium. Then, we reset the parameter to its initial value and obtain a third equilibrium. We compared the wavelengths of the first and third equilibria. Observing the same wavelength would mean that the system exactly recovers its initial state.

Figure 8 shows that large differences in wavelength can be observed between the first and third equilibria, with both feedbacks. The strain feedback, however, is not as sensitive, compare the left and right columns in Fig. 8. This is qualitatively consistent with its lower sensitivity to noise, documented in the previous subsection.

3 Discussion

We developed here a mechanochemical model for auxin patterning in the plant shoot apical meristem. The central question, addressed with our model, is whether the insertion of the efflux facilitators (transporters) in the membrane depends on the strain of the cell walls or by the stress applied to them. To this end, we compared the predictions of the model with available experimental results.

We found that both stress- and strain-based feedbacks lead to similar predictions when simulating cell ablation, turgor-induced changes in tissue tension or a global reduction of the stiffness of the cell walls, generally in agreement with observations. Modeling *PMEI*-overexpressing plants allowed us to discriminate between the two models: Assuming that auxin effect on cell wall stiffness is reduced in such plant lines, we found that only the strain-based feedback directly accounted for observations. Interestingly, organogenesis is abolished in these lines, showing that it is useful to study the system behavior in the absence of patterns. We also compared patterns of auxin and PIN1 concentrations and show both numerically and analytically that only a strain-sensing mechanism can explain their correlation, as observed in incipient primordia, whereas a stress-sensing mechanism leads to anti-correlated patterns. Note that we assume the amount of transporters per cell to be constant, whereas experiments show that the application of auxin increases PIN1 concentration (Heisler et al. 2005). Although we cannot rule out that this effect compensates for the observed anti-correlation with a stress-based feedback, a strain-sensing mechanism seems more plausible. Finally, investigating the effect of noise, or of a transient change in chemical parameters, on patterning strengthened our conclusion: Patterns appear more robust with the strain-based feedback.

The model, however, partly failed to reproduce the observations concerning the effect of tissue tension on polarity. Irrespective of the feedback chosen, we found that polarity increased with tension, whereas experimentally, polarity slightly decreases from isotonic to hypertonic conditions (Nakayama et al. 2012). Again, a possible explanation is that we assumed the amount of transporters per cell to be constant, whereas PIN1 levels decrease in hypertonic conditions; other processes might be triggered when plants react to such osmotic stress. Alternatively, the slight decrease observed could be due to a small experimental bias, and the difference between experiments and our simulations may not be very significant. In addition, the model yielded wavelengths that were smaller for stress-sensing than for strain-sensing. As we have found no explanation for this difference, it is difficult to know whether the model is incomplete or whether this result would also favor strain-sensing because auxin peaks are observed to have a smaller spatial extent than inter-peak distance, which resembles more simulated strain-sensing (Fig. 1c, right). Because of this difference in wavelength, we also explored other values of parameters for the stress-based feedback and found that all conclusions on the comparison with the strain-based feedback hold, except for the conclusions on robustness that are more sensitive to parameter values (supplementary text, Figures S2–S7).

The idealized hexagonal geometry of the cells and the absence of tissue growth are important limitations of the model. The agreement of the analytical linear stability analysis with simulations (supplementary text, Figure S1) makes it likely that cell topology has little effect on our conclusions. Nevertheless, plants respond to mechanical stimuli by altering their growth rates (Moullia et al. 2015). Increase in auxin levels induces cell growth (Braybrook and Peaucelle 2013), which induces tissue reorganization, changes in mechanical stress (Alim 2012) and ultimately feeds back on auxin transport. Although these processes are important in development, mechanical signals are quasi-instantaneous and mostly depend on the current state of the tissue, so that we do not expect them to significantly change our main conclusions.

Altogether, our results favor a feedback based on strain, though many of the experimental configurations are insensitive to whether the mechanical feedback on auxin transport is provided by stress or strain. This raises the question of the underlying molecular mechanisms. Many types of mechanosensors are known (Pruitt et al. 2014). In the case of PIN1, strain could shift the balance between endocytosis and exocytosis, accounting for the strain-based feedback, because osmotic stress affects cell trafficking, in particular through clathrin-mediated endocytosis (Zwiewka et al. 2015). The contact between the plasma membrane and the cell wall is needed for PIN1 polarity (Boutté et al. 2006; Feraru et al. 2011), suggesting that the mechanical state of the cell wall is relevant for polarity. However, the role of the cell wall might just be to reduce lateral diffusion of PIN1, helping to maintain the distribution of PIN1 determined by cell trafficking (Martinière et al. 2012).

The question of strain- and stress-sensing was raised in the different, but related, context of plant cortical microtubules orientation by mechanical cues, and the combination of experimental and theoretical approaches suggests that stress-sensing is more likely to be involved (Hamant et al. 2008; Bozorg et al. 2014). The same conclusion has been reached concerning the actomyosin cortex in the drosophila wing disc (Legoff et al. 2013). However, the case of isolated animal cells has been debated. Early exper-

iments suggested force-sensing (Freyman et al. 2002) or deformation-sensing (Saez et al. 2005). More recent experiments showed that deformation-sensing occurred at low force, while force-sensing occurred at high force (Yip et al. 2013), though other experiments showed that cells could sense the stiffness of extracellular space (Mitrossilis et al. 2010), consistently with the observation that cells can differentiate according to the stiffness of their environment (Bellas and Chen 2014). Actually, mechanosensing occurs at different scales (Pruitt et al. 2014), so that the mechanical variable sensed may depend on the sensing molecule and on the specific function associated with sensing.

In order to disentangle the parameters involved in mechanosensing, it is necessary to combine experimental perturbations of cells or tissues with analytical and computational studies of their behaviors. This is now made possible by the improvement of micromechanical (Milani et al. 2013) and computational (Chickarmane et al. 2010) approaches. In this spirit, the present work provides insight on how the interaction between biomechanical and biochemical fields may contribute to the robustness of morphogenesis.

Model Formulation

Tissue mechanics We describe here in details the model summarized in Fig. 1. We only consider auxin transport through anticlinal cell walls in the epidermis, and thus, we neglect the mechanical contribution of other cell walls. We assume the rest state of the tissue to be a regular hexagonal tiling of the plane and we formulate the problem in terms of a vertex model with periodic boundary conditions. The equilibrium positions of the vertices are obtained by minimizing the mechanical energy of the N_C cells. The contribution to the mechanical energy of the cell wall common to adjacent cells i and j has a linear density

$$E_{i,j} = \frac{1}{2}k_{i,j}\varepsilon_{i,j}^2; \varepsilon_{i,j} = \frac{l_{i,j} - l^{(0)}}{l^{(0)}},$$

where $k_{i,j}$ is the stiffness of this wall, $l_{i,j}$ its length (with an equilibrium value equal to $l^{(0)}$), and $\varepsilon_{i,j}$ its strain. The stress in the anticlinal wall is then given by the derivative of its energy with respect to strain:

$$S_{i,j} \equiv \frac{\partial E_{i,j}}{\partial \varepsilon_{i,j}}.$$

The forces resulting from turgor pressure and tissue curvature are accounted for by external stress with components σ_x , σ_y . The total energy of the tissue then takes the form

$$E = -\sigma_x L_y^{(0)} (L_x - L_x^{(0)}) - \sigma_y L_x^{(0)} (L_y - L_y^{(0)}) + \sum_{(i,j)} l^{(0)} E_{i,j} \quad (1)$$

where L_x and L_y are the tissue dimensions along the x and y directions and $L_x^{(0)}$ and $L_y^{(0)}$ their values without external stress; the sum is over the pairs of neighboring cells (i, j) . Here, we considered only the case of isotropic stress, such that $\sigma_x = \sigma_y = \sigma$.

Auxin dynamics and coupling with the mechanics We use the same assumptions as in previous studies (Jönsson et al. 2006; Sahlin et al. 2009). Namely, we only model auxin concentrations in the cytosol. We also assume that PIN1 dynamics occurs with a timescale that is shorter than the time necessary for the transport of auxin through cell walls. The latter is therefore the limiting step. These assumptions allow us to reduce the model to only one chemical equation that describes the auxin concentration, a_i , in cell i :

$$\frac{da_i}{dt} = s_a - d_a a_i - \frac{P}{A} \sum_{\langle j \rangle_i} l_{i,j} (t(a_i) p_{i,j} - t(a_j) p_{j,i}) - \frac{D}{A} \sum_{\langle j \rangle_i} l_{i,j} (a_i - a_j), \quad (2)$$

where s_a is auxin synthesis rate, d_a is auxin degradation rate, and D is the diffusion coefficient. $\langle j \rangle_i$ is the set of indices of the six cells adjacent to cell i . We assume elastic strain to be small, so that the area of each cell is approximated by its rest area A . The total amount of PIN1 proteins per cell, $P \sum_{\langle j \rangle_i} l_{i,j}$, is assumed to be cell-independent;

$p_{i,j}$ is the normalized linear concentration of PIN1 proteins localized at the membrane of cell i and facing cell j . (This PIN1 fraction is responsible for auxin efflux from cell i to cell j ; P is used as a unit of linear concentrations.) The rate of auxin transport by PIN1 proteins, $t(a)$, has the following sigmoidal-dependence on auxin concentration:

$$t(a) = \frac{a^{H_t}}{K_t^{H_t} + a^{H_t}}$$

where K_t is a threshold in auxin concentration and H_t the Hill exponent.

Auxin controls tissue mechanics by softening the cell walls (Fig. 1). The stiffness of the walls decreases with the amount of auxin in the cells:

$$k_{i,j}(a_i) = k_{\min} + \delta k \frac{K_k^{H_k}}{K_k^{H_k} + a_i^{H_k}} \quad (3)$$

where k_{\min} is the wall stiffness in the absence of auxin, δk the variations in stiffness, K_k the auxin threshold, and H_k the Hill exponent.

The mechanical effects on the cell also affect auxin dynamics via its transport. The amount of PIN1 transporters in a cell membrane is affected by the strain or the stress, as illustrated in Fig. 1a. The normalized concentration, $p_{i,j}$, of PIN1 proteins localized at the plasma membrane of cell i and facing cell j reads

Table 1 Values of the parameters used in the simulation: Parameters were estimated from previous models (Jönsson et al. 2006; Sahlin et al. 2009; Heisler et al. 2010). Stiffness dependence on auxin concentration was chosen to display fivefold variations, in the range of realistic values (Milani et al. 2011). The tension resulting from hydrostatic pressure was then chosen to yield a typical deformation of 4%, in the range estimated from osmotic treatments (Nakayama et al. 2012). Finally, PIN1 insertion was tuned so that the fraction of transporters inserted in the membrane is around 0.7, similar to experimental estimates (Nakayama et al. 2012)

$l^{(0)}$	σ	s_a	d_a	D	P	K_t	H_t	K_f	H_f	k_0	k_{\min}	δk	K_k	H_k
1	1.4	1	0.5	5	100	2	1	30	3	30	10	40	2	2

$$p_{i,j} = \frac{K_f^{H_f} \left(\left(\alpha + (1 - \alpha) \frac{k_{i,j}}{k_0} \right) \varepsilon_{i,j} \right)^{H_f}}{1 + \frac{\sum_{\langle k \rangle_i} l_{i,k} K_f^{H_f} \left(\left(\alpha + (1 - \alpha) \frac{k_{i,k}}{k_0} \right) \varepsilon_{i,k} \right)^{H_f}}{\sum_{\langle k \rangle_i} l_{i,k}}}$$

where $\alpha = 0$ for the stress feedback, $\alpha = 1$ for the strain feedback, and $\varepsilon_{i,j}$ and $k_{i,j}$ stand for wall strain and wall stiffness as described above. The parameter k_0 is set to k^* , the value of the stiffness in the homogeneous equilibrium state, so that the contributions of stress and strain are of the same order of magnitude in the homogeneous state. K_f sets the amplitude of the insertion function, and H_f is the corresponding exponent.

Observables Two observables are relevant for the comparison between our simulations and experimental observations, see Fig. 1b (Nakayama et al. 2012; Braybrook and Peaucelle 2013). The first is polarity, defined as the ratio of the PIN1 concentrations on the most and least enriched membrane of cell i :

$$\mathcal{P}_i = \frac{p_i^{\max}}{p_i^{\min}} = \frac{\max_{\langle j \rangle_i} (p_{i,j})}{\min_{\langle j \rangle_i} (p_{i,j})},$$

and the second is the ratio of plasma membrane-localized PIN1 to the total amount in the cell:

$$\mathcal{F}_i = \frac{P_i^{\text{wall}}}{P_i^{\text{in}} + P_i^{\text{wall}}} = \frac{\sum_{\langle j \rangle_i} l_{i,j} p_{i,j}}{\sum_{\langle j \rangle_i} l_{i,j}}.$$

P does not appear in this equation because it was used to normalize $p_{i,j}$. In practice, we note \mathcal{P} and \mathcal{F} their distribution over the tissue.

Implementation The model was programmed in C. The mechanical energy 1 is minimized thanks to the BFGS algorithm (Luksan 2001), implemented in the NLOpt library (Johnson 2008). The differential equations for the auxin concentration 2 are solved iteratively thanks to the GNU GSL library with a Runge–Kutta (2, 3) method

(Gough 2009). We assume that the typical timescale to reach the mechanical equilibrium is much smaller than the timescale for auxin regulation. Consequently, we compute the evolution of the system iteratively, by first computing the evolution of the auxin concentration on a small time-step, and updating the configuration of the tissue by minimizing its mechanical energy. The time-step $dt = 0.1$ for the evolution of auxin dynamics was chosen to limit the number of energy minimizations while generating the same results than smaller values. The code is available on Github (github.com/JeanDanielJulien/auxinTransport). Simulations results were analyzed, and figures were made with Matlab. Table 1 summarizes the values of the parameters used in the present work.

Acknowledgements This work was supported by the Human Frontier Science Program (RGP0008/2013) and the ANR MechInMorph (ANR-12-BSV2-0023) to AB.

References

- Adler I, Barabe D, Jean RV (1997) A history of the study of phyllotaxis. *Ann Bot* 80(3):231–244
- Alim K (2012) Regulatory role of cell division rules on tissue growth heterogeneity. *Front Plant Sci*. <https://doi.org/10.3389/fpls.2012.00174>
- Bellas E, Chen CS (2014) Forms, forces, and stem cell fate. *Curr Opin Cell Biol* 31C:92–97. <https://doi.org/10.1016/j.ccb.2014.09.006>
- Bode HR (2009) Axial patterning in hydra. *Cold Spring Harbor Perspect Biol* 1(1):a000,463–a000,463. <https://doi.org/10.1101/cshperspect.a000463>
- Boutté Y, Crosnier MT, Carraro N, Traas J, Satiat-Jeunemaitre B (2006) The plasma membrane recycling pathway and cell polarity in plants: studies on pin proteins. *J Cell Sci* 119(Pt 7):1255–65. <https://doi.org/10.1242/jcs.02847>
- Bozorg B, Krupinski P, Jönsson H (2014) Stress and strain provide positional and directional cues in development. *PLoS Comput Biol* 10(1):e1003,410. <https://doi.org/10.1371/journal.pcbi.1003410>
- Braybrook SA, Peaucelle A (2013) Mechano-chemical aspects of organ formation in *Arabidopsis thaliana*: the relationship between auxin and pectin. *PLoS ONE* 8(3):e57,813. <https://doi.org/10.1371/journal.pone.0057813>
- Chickarmane V, Roeder AH, Tarr PT, Cunha A, Tobin C, Meyerowitz EM (2010) Computational morphodynamics: a modeling framework to understand plant growth. *Ann Rev Plant Biol* 61(1):65–87. <https://doi.org/10.1146/annurev-arplant-042809-112213>
- Davidson LA (2011) Embryo mechanics balancing force production with elastic resistance during morphogenesis. *Curr Top Dev Biol* 95:215–41. <https://doi.org/10.1016/B978-0-12-385065-2.00007-4>
- Feraru E, Feraru MI, Kleine-Vehn J, Martinière A, Mouille G, Vanneste S, Vernhettes S, Runions J, Friml J (2011) Pin polarity maintenance by the cell wall in arabidopsis. *Curr Biol CB* 21(4):338–43. <https://doi.org/10.1016/j.cub.2011.01.036>
- Fernández-Sánchez ME, Barbier S, Whitehead J, Béalle G, Michel A, Latorre-Ossa H, Rey C, Fouassier L, Claperton A, Brullé L, Girard E, Servant N, Rio-Frio T, Marie H, Lesieur S, Housset C, Gennisson JL, Tanter M, Ménager C, Fre S, Robine S, Farge E (2015) Mechanical induction of the tumorigenic-catenin pathway by tumour growth pressure. *Nature* 523(7558):92–5. <https://doi.org/10.1038/nature14329>
- Freyman TM, Yannas IV, Yokoo R, Gibson LJ (2002) Fibroblast contractile force is independent of the stiffness which resists the contraction. *Exp Cell Res* 272(2):153–62. <https://doi.org/10.1006/excr.2001.5408>
- Geitmann A, Ortega JK (2009) Mechanics and modeling of plant cell growth. *Trends Plant Sci* 14(9):467–478. <https://doi.org/10.1016/j.tplants.2009.07.006>
- Gough B (2009) GNU scientific library reference manual, 3rd edn. Network Theory Ltd, London
- Hamant O, Heisler MG, Jönsson H, Krupinski P, Uyttewaal M, Bokov P, Corson F, Sahlin P, Boudaoud A, Meyerowitz EM (2008) Others: developmental patterning by mechanical signals in Arabidopsis. *Science* 322(5908):1650–1655. <http://science.sciencemag.org/content/322/5908/1650.long>

- Hamant O, Traas J (2010) The mechanics behind plant development. *New Phytol* 185(2):369–385. <https://doi.org/10.1111/j.1469-8137.2009.03100.x>
- Heisler MG, Ohno C, Das P, Sieber P, Reddy GV, Long JA, Meyerowitz EM (2005) Patterns of auxin transport and gene expression during primordium development revealed by live imaging of the Arabidopsis inflorescence meristem. *Curr Biol* 15(21):1899–1911. <https://doi.org/10.1016/j.cub.2005.09.052>
- Heisler MG, Hamant O, Krupinski P, Uyttewaal M, Ohno C, Jönsson H, Traas J, Meyerowitz EM (2010) Alignment between PIN1 polarity and microtubule orientation in the shoot apical meristem reveals a tight coupling between morphogenesis and auxin transport. *PLoS Biol* 8(10):e1000516. <https://doi.org/10.1371/journal.pbio.1000516>
- Howard J, Grill SW, Bois JS (2011) Turing's next steps: the mechanochemical basis of morphogenesis. *Nat Rev Mol Cell Biol* 12(6):400–6. <https://doi.org/10.1038/nrm3120>
- Iskratsch T, Wolfenson H, Sheetz MP (2014) Appreciating force and shape—the rise of mechanotransduction in cell biology. *Nat Rev Mol Cell Biol*. <https://doi.org/10.1038/nrm3903>
- Johnson SG (2008) The NLOpt nonlinear-optimization package. [https://nlopt.readthedocs.io/en/latest/cell.com/trends/plant-science/fulltext/S1360-1385\(07\)00058-1](https://nlopt.readthedocs.io/en/latest/cell.com/trends/plant-science/fulltext/S1360-1385(07)00058-1)
- Jönsson H, Heisler MG, Shapiro BE, Meyerowitz EM, Mjolsness E (2006) An auxin-driven polarized transport model for phyllotaxis. *Proc Natl Acad Sci U S A* 103(5):1633–1638. <https://www.pnas.org/content/103/5/1633.short>
- Kondo S (2002) The reaction–diffusion system: a mechanism for autonomous pattern formation in the animal skin. *Genes Cells* 7(6):535–541. <https://doi.org/10.1046/j.1365-2443.2002.00543.x>
- Kuhlemeier C, Reinhardt D (2001) Auxin and phyllotaxis. *Trends Plant Sci* 6(5):187–189. [https://www.cell.com/trends/plant-science/fulltext/S1360-1385\(07\)00058-1](https://www.cell.com/trends/plant-science/fulltext/S1360-1385(07)00058-1)
- Legoff L, Rouault H, Lecuit T (2013) A global pattern of mechanical stress polarizes cell divisions and cell shape in the growing drosophila wing disc. *Development* 140(19):4051–9. <https://doi.org/10.1242/dev.090878>
- Luksan L (2001) New subroutines for large-scale optimization. <http://www.cs.cas.cz/~luksan/subroutines.html>
- Martinière A, Lavagi I, Nageswaran G, Rolfe DJ, Maneta-Peyret L, Luu DT, Botchway SW, Webb SED, Mongrand S, Maurel C, Martin-Fernandez ML, Kleine-Vehn J, Friml J, Moreau P, Runions J (2012) Cell wall constrains lateral diffusion of plant plasma-membrane proteins. *Proc Natl Acad Sci U S A*. <https://doi.org/10.1073/pnas.1202040109>
- Milani P, Gholamirad M, Traas J, Arnodo A, Boudaoud A, Argoul F, Hamant O (2011) In vivo analysis of local wall stiffness at the shoot apical meristem in Arabidopsis using atomic force microscopy: measuring wall stiffness in meristems with AFM. *Plant J* 67(6):1116–1123. <https://doi.org/10.1111/j.1365-313X.2011.04649.x>
- Milani P, Braybrook SA, Boudaoud A (2013) Shrinking the hammer: micromechanical approaches to morphogenesis. *J Exp Bot* 64(15):4651–62. <https://doi.org/10.1093/jxb/ert169>
- Mitrossilis D, Fouchard J, Pereira D, Postic F, Richert A, Saint-Jean M, Asnacios A (2010) Real-time single-cell response to stiffness. *Proc Natl Acad Sci U S A*. <https://doi.org/10.1073/pnas.1007940107>
- Moulija B, Coutand C, Julien JL (2015) Mechanosensitive control of plant growth: bearing the load, sensing, transducing, and responding. *Front Plant Sci*. <https://doi.org/10.3389/fpls.2015.00052>
- Nakayama N, Smith RS, Mandel T, Robinson S, Kimura S, Boudaoud A, Kuhlemeier C (2012) Mechanical regulation of auxin-mediated growth. *Curr Biol* 22(16):1468–1476. <https://doi.org/10.1016/j.cub.2012.06.050>
- Newell AC, Shipman PD, Sun Z (2008) Phyllotaxis: cooperation and competition between mechanical and biochemical processes. *J Theor Biol* 251(3):421–439. <https://doi.org/10.1016/j.jtbi.2007.11.036>
- Okada K, Ueda J, Komaki MK, Bell CJ, Shimura Y (1991) Requirement of the auxin polar transport system in early stages of Arabidopsis floral bud formation. *Plant Cell* 3(7):677–684. <https://doi.org/10.1105/tpc.3.7.677>
- Palme K, Gälweiler L (1999) PIN-pointing the molecular basis of auxin transport. *Curr Opin Plant Biol* 2(5):375–381. [https://doi.org/10.1016/S1369-5266\(99\)00008-4](https://doi.org/10.1016/S1369-5266(99)00008-4)
- Peaucelle A, Louvet R, Johansen JN, Hfte H, Laufs P, Pelloux J, Mouille G (2008) Arabidopsis phyllotaxis is controlled by the methyl-esterification status of cell-wall pectins. *Curr Biol* 18(24):1943–1948. <https://doi.org/10.1016/j.cub.2008.10.065>
- Peaucelle A, Braybrook SA, Guillou LL, Bron E, Kuhlemeier C, Höfte H (2011) Pectin-induced changes in cell wall mechanics underlie organ initiation in arabidopsis. *Curr Biol CB*. <https://doi.org/10.1016/j.cub.2011.08.057>

- Pruitt BL, Dunn AR, Weis WI, Nelson WJ (2014) Mechano-transduction: from molecules to tissues. *Plos Biol* 12(11):e1001996. <https://doi.org/10.1371/journal.pbio.1001996>
- Rauzi M, Lenne PF (2011) Cortical forces in cell shape changes and tissue morphogenesis. *Curr Top Dev Biol* 95:93–144. <https://doi.org/10.1016/B978-0-12-385065-2.00004-9>
- Reinhardt D, Mandel T, Kuhlemeier C (2000) Auxin regulates the initiation and radial position of plant lateral organs. *Plant Cell* 12(4):507–518. <https://doi.org/10.1105/tpc.12.4.507>
- Reinhardt D, Pesce ER, Stieger P, Mandel T, Baltensperger K, Bennett M, Traas J, Friml J, Kuhlemeier C (2003) Regulation of phyllotaxis by polar auxin transport. *Nature* 426(6964):255–260. <https://doi.org/10.1038/nature02081>
- Ryden P, Sugimoto-Shirasu K, Smith AC, Findlay K, Reiter WD, McCann MC (2003) Tensile properties of arabidopsis cell walls depend on both a xyloglucan cross-linked microfibrillar network and rhamnogalacturonan ii-borate complexes. *Plant Physiol* 132(2):1033–40. <https://doi.org/10.1104/pp.103.021873>
- Saez A, Buguin A, Silberzan P, Ladoux B (2005) Is the mechanical activity of epithelial cells controlled by deformations or forces? *Biophys J* 89(6):L52–4. <https://doi.org/10.1529/biophysj.105.071217>
- Sahlin P, Sderberg B, Jönsson H (2009) Regulated transport as a mechanism for pattern generation: capabilities for phyllotaxis and beyond. *J Theor Biol* 258(1):60–70. <https://doi.org/10.1016/j.jtbi.2009.01.019>
- Sampathkumar A, Yan A, Krupinski P, Meyerowitz EM (2014) Physical forces regulate plant development and morphogenesis. *Curr Biol* 24(10):R475–R483. <https://doi.org/10.1016/j.cub.2014.03.014>
- Sassi M, Ali O, Boudon F, Cloarec G, Abad U, Cellier C, Chen X, Gilles B, Milani P, Friml J, Vernoux T, Godin C, Hamant O, Traas J (2014) An auxin-mediated shift toward growth isotropy promotes organ formation at the shoot meristem in Arabidopsis. *Curr Biol* 24(19):2335–2342. <https://doi.org/10.1016/j.cub.2014.08.036>
- Smith RS, Bayer EM (2009) Auxin transport-feedback models of patterning in plants. *Plant Cell Environ* 32(9):1258–1271. <https://doi.org/10.1111/j.1365-3040.2009.01997.x>
- Smith RS, Guyomarc'h S, Mandel T, Reinhardt D, Kuhlemeier C, Prusinkiewicz P (2006) A plausible model of phyllotaxis. *Proc Natl Acad Sci U S A* 103(5):1301–1306. <https://doi.org/10.1073/pnas.0510457103>
- Stoma S, Lucas M, Chopard J, Schaedel M, Traas J, Godin C (2008) Flux-based transport enhancement as a plausible unifying mechanism for auxin transport in meristem development. *PLoS Comput Biol* 4(10):e1000207. <https://doi.org/10.1371/journal.pcbi.1000207>
- Vernoux T, Kronenberger J, Grandjean O, Laufs P, Traas J (2000) PIN-FORMED 1 regulates cell fate at the periphery of the shoot apical meristem. *Development* 127(23):5157–5165. <http://dev.biologists.org/content/127/23/5157.short>
- Vernoux T, Brunoud G, Farcot E, Morin V, Van Den Daele H, Legrand J, Oliva M, Das P, Larrieu A, Wells D, Guédon Y, Armitage L, Picard F, Guyomarc'h S, Cellier C, Parry G, Koumproglou R, Doonan JH, Estelle M, Godin C, Kepinski S, Bennett M, De Veylder L, Traas J (2011) The auxin signalling network translates dynamic input into robust patterning at the shoot apex. *Mol Syst Biol* 7:508. <https://doi.org/10.1038/msb.2011.39>
- Yip AK, Iwasaki K, Ursekar C, Machiyama H, Saxena M, Chen H, Harada I, Chiam KH, Sawada Y (2013) Cellular response to substrate rigidity is governed by either stress or strain. *Biophys J* 104(1):19–29. <https://doi.org/10.1016/j.bpj.2012.11.3805>
- Zwiewka M, Nodzyński T, Robert S, Vanneste S, Friml J (2015) Osmotic stress modulates the balance between exocytosis and clathrin-mediated endocytosis in Arabidopsis thaliana. *Mol Plant* 8(8):1175–87. <https://doi.org/10.1016/j.molp.2015.03.007>

Affiliations

Jean-Daniel Julien^{1,2,3}  · **Alain Pumir**^{1,2,3}  · **Arezki Boudaoud**¹ 

¹ Reproduction et Développement des Plantes, ENS de Lyon, UCB Lyon 1, CNRS, INRA, Université de Lyon, Lyon Cedex 07, France

² Laboratoire de Physique, ENS de Lyon, UCB Lyon 1, CNRS, Université de Lyon, Lyon Cedex 07, France

³ Max-Planck Institute for Dynamics and Self-Organization, 37077 Göttingen, Germany